Preparation of Illite Coated Geomaterial Microfluidic Surfaces: Effect of Salinity and Heat Treatment

Rupom Bhattacherjee, Prem K. Bikkina*

School of Chemical Engineering, Oklahoma State University, 420 Engineering North, Stillwater, 74078

*Corresponding author: *prem.bikkina@okstate.edu*

Email addresses: rupom.bhattacherjee@okstate.edu (Rupom Bhattacherjee, prem.bikkina@okstate.edu (Prem K. Bikkina).

1 Abstract

Unique characteristics of clay (e.g., high surface area, deficiency in positive charges) make any clay abundant shales a good source of adsorbed gas. However, the presence of clay in porous media can also affect shale rock's producibility. The clay-water interaction can cause significant swelling and fines migration in the formation and impair the overall hydrocarbon recovery from shale.

Geomaterial micromodels, developed by functionalizing traditional glass or PDMS surfaces with geomaterials (e.g., calcite, Quartz, clay), can represent the physicochemical properties of the natural porous media and have been used during the last few years to understand and evaluate the solid-fluid physicochemical interactions. This study focuses on developing a clay-coated geomaterial surface and investigates the effect of base fluid's salinity on clay adsorption to the glass surface. Glass capillary tubes and straight channel borosilicate glass micromodels are coated with Illite clay to represent the pore-scale clay chemistry of Caney Shale, a Mississippian unconventional play in Southern Oklahoma, USA. 10 wt.% of Illite clay slurries made with brines of four different salinities are used to coat the glass-capillary tubes to understand the effect of salinity in clay adsorption on the glass surface and overall coating quality. To achieve a stable coating and evaluate the impact of heat treatment on coating's stability, straight channel glass flow cells coated with Illite clay are heat-treated at low (25 °C) and high temperature (125 °C), and the results are compared with an untreated coated surface. Flooding tests were carried out with brines of different salinities on the coated surface to evaluate the stability of the coating.

The experimental results indicated a strong relationship between the brine's salinity and the adsorption of clay particles on the glass surface. An increase in brine concentration resulted in improved adsorption of clay particles on the glass surface. Experiments involving heat treating

the glass surface following the coating demonstrated significant improvement in the stability of the coating.

2 Introduction

Clay minerals account for, on average, 60 wt.% of most shales (Shaw and Weaver, 1965). It is generally agreed that the presence of clay in a shale formation can significantly affect fluid flow through the ultra-low permeability porous media. This may lead to a severe reduction in the production rate even after hydraulic fracturing (Rahman et al., 2007). This is mainly due to the swelling induced in clay as a result of the interaction between injected water and clay minerals, resulting in reduced pore space and permeability.

Different clay minerals have different levels of swelling potential depending on their structural composition and cation exchange capacity (CEC) (Muhammed et al., 2021). Smectite having a larger surface area and higher CEC than other common clay minerals, such as Kaolinite and Illite, demonstrate greater affinity to adsorb water into the formation, followed by significant swelling (Murray, 2006; Rogala et al., 2013). Kaolinite is a 1:1 silicate mineral where one tetrahedral unit is linked through an oxygen atom with another octahedral unit. Because each tetrahedron-octahedron layer (T-O) in Kaolinite is connected with Van der Waals force and a strong hydrogen bond, Kaolinite is a non-swelling clay. In contrast, Illite is a 2:1 clay mineral where one octahedral sheet is squeezed between two tetrahedral units (T-O-T). Illite has potassium ions fitted into the interlayer region, preventing water encroachment into the region. This is why Illite is less sensitive to swelling. However, in the case of Smectite, each T-O-T layer is connected with another T-O-T layer with a weak Van der Waals force. Therefore, water can easily encroach between the layers, making Smectite a highly expandable clay (Grim, 1953; Liu and Lu, 2006).

Clay swelling increases with the decrease in brine salinity as the double-layer spacing between the clay molecules expands when they encounter brines of less ionic strength. Montmorillonite clay is reported to be swelled by 30% in diameter once 5000 mg/L NaCl brine is replaced by pure water (Zhuang et al., 2018). Fang et al. (2017) studied the sensitivity of clay-containing core samples to brines of different salinities. They observed a significant swelling-induced permeability reduction in the porous media once the injection fluid was changed from formation water with 9662.9 mg/L salinity to pure water.

Fines migration is another phenomenon that can significantly affect shales' productivity. Detachment of the fines from the surface can be induced by hydrodynamic and colloidal forces. Hydrodynamic forces depend on parameters such as fluid velocity, flow dimension, and particle size. A sensitivity study conducted by Tangparitkul et al. (2020) revealed that, under the influence of effective stress, particle size and fluid velocity are the dominant parameters that affect the hydrodynamic forces and control the fines migration.

In the presence of swelling clay (e.g., smectite), the salinity of brines may also influence the hydrodynamic forces and cause fines migration. Exposure to brines of salinity less than the critical salt concentration (CSC) may cause the clayey formation to swell and reduce the dimension of the flow channel. Narrowed pore space creates obstruction in the fluid flow, exerts fluid force on the pore wall, and promotes particle detachment (Song and Kovscek, 2016; Tangparitkul et al., 2020; Wilson et al., 2014).

Conversely, colloidal forces are sourced from the net effect of London-van der Waals attractive (vdW) forces and electric double layer (EDL) repulsive forces between the clay particles and rock surfaces. The van der Waals forces retain the clay particles on the grain surface, while EDL

forces are responsible for the detachment and migration of the particles in the porous media (Israelachvili, 2011; Khilar and Fogler, 1998; Tchistiakov, 2000).

In the presence of high salinity formation brine, clay particles are attached to the pore wall mainly by the influence of the vdW forces between clay particles and the pore surface. As the brine salinity starts to decrease due to the injection of low salinity brines or freshwater, the net forces binding the clay particles to the pore wall start to diminish, and when the salinity is below CSC, the repulsive EDL forces start to dominate the colloidal force, and the fines get detached from the surface (Mohan and Fogler, 1997; Muneer et al., 2020). Khilar and Fogler (1984) reported a significant reduction in the permeability of Berea sandstone due to the release of clay particles from the grain surface when the salinity of permeating fluid was below the critical level. Permeability reduction due to the release of the clay particles upon exposure to low salinity injection fluids was also confirmed by many other researchers (Cihan et al., 2022; Han et al., 2020; Sarkar and Sharma, 1990; Song and Kovscek, 2016; Zeinijahromi et al., 2011).

Pang and Liu (2013) measured the permeability loss in sand-pack filled with unconsolidated sand when steam and condensate of low salinity and high temperature were injected into the porous media. Their experimental results revealed an irreversible reduction of permeability up to 43.52% due to particle migration and hydrothermal reactions caused by steam and its condensate with formation minerals.

Wilson et al. (2014) critically reviewed the clay mineralogy of sandstone reservoirs in the North Sea and reported the breakup of Kaolinite aggregates and mobilization of Illite clay particles during fluid injection as the probable cause of formation damage in the North Sea sandstones.

In addition to the ionic effects of brines, the hydrodynamic forces exerted by the injection fluid can further aid the detachment of clay particles from the surface. However, Ochi and Vernoux (1998) observed that chemical effects resulting from the non-compatibility between injected fluid and clay in the sandstone formation caused more reduction in the formation permeability compared to hydrodynamic effects of flow.

Clay swelling can also cause surface roughening and alters the wettability of the pores in favor of additional oil recovery during low salinity water flooding (Marhaendrajana et al., 2018). Ridwan et al. (2020) explored the implications of surface roughening and pore size alteration generated from the swelling of the Kaolinite, Montmorillonite, and Muscovite clays at various brine conditions. Low salinity brines with monovalent ions significantly reduced the pore size and resulted in lower recovery for the high clay content cores. However, when the clay content was low, the monovalent ions actually promoted oil recovery. They attributed this effect to the change in wettability due to surface roughening from clay swelling. When the clay content was high, the effect of pore size alteration took over the effect of wettability alteration and reduced oil recovery.

Different laboratory tests, such as dispersion test, immersion test, bulk hardness test, etc., are developed to study the effects of rock-fluid interactions (Stephens et al., 2009). However, these tests are designed to assess rock samples' stability upon exposure to different fluids by immersing them in the fluids (Gomez and He, 2012) or flowing the fluids through them (Sayegh et al., 1990; Somerton and Radke, 1983). Since rock samples are usually composed of more than one mineral (Quartz, calcite, clay, etc.), these tests can not recognize the potential clay-fluid interaction and its impact on formation damage. Moreover, these test results do not reflect the in-

situ behavior of clay upon exposure to any fluids, nor do they provide any pore-scale visualizations of the rock-fluid interaction.

Geomaterial functionalized microfluidic chip, developed by coating traditional micromodels, a substrate usually made with glass, Quartz, or any transparent materials that facilitates visual observation of flow network, with any geomaterials, is an excellent tool that can be facilitated with the required level of surface heterogeneity and surface chemistry to represent the pore-scale flow dynamics. They also provide the ability to mimic specific surface mineralogy of any rock and facilitate visual observation of the surface's behavior upon exposure to various fluids. Besides, the micromodel flow networks are highly customizable (Campbell and Orr, 1985) and provide easy and accurate control of fluid flow (Karadimitriou and Hassanizadeh, 2012).

Geomaterial micromodels have been used in the last few years to mimic porous media and study various fundamental and applied aspects of multiphase flow such as wettability alteration (Grattoni and Dawe, 2003; Khajepour et al., 2014; Laroche et al., 1999; Saadat et al., 2021; Yekeen et al., 2020), interfacial tension (Mackay et al., 1998; Xu et al., 2022), capillary pressure (Ghazanfari et al., 2007; Smith et al., 2005), and formation damage (Mohammadalinejad et al., 2019; Onaka and Sato, 2021; Sharifipour et al., 2019).

Researchers have also used micromodels to explore the mechanisms of different enhanced oil recovery (EOR) methods (Gaol et al., 2021; Mehdizad et al., 2022; Seyyedi et al., 2018; Su et al., 2022; Sun et al., 2021). Low salinity water flooding (LSWF) is one of the EOR methods we observed been investigated the most using geomaterial micromodels.

Song and Kovscek (2015, 2016) functionalized glass micromodels with clay minerals to study the effect of pore-scale fines migration and formation damage in the low salinity oil recovery

process. Amirian et al. (2017) also performed a detailed study on pore-scale displacement process during LSWF. Their study incorporated two-dimensional clay-coated oil-wet and water-wet micromodels to visually study the role of wettability alteration, snap-off, and fines migration in the dynamic displacement of oil during flooding.

A similar study was performed by Mohammadi and Mahani (2020) for carbonates (Mohammadi and Mahani, 2020) and Shahmohammadi et al. (2021) for sandstones to investigate the low salinity oil recovery process. Mohammadi and Mahani (2020) postulated the presence of an initial water film (connate water) in facilitating the diffusive transportation of low salinity brine and enhancing the potential of LSWF for carbonates, while Shahmohammadi et al. (2021) reported a critical brine salinity below which polar components of oil start to break and formulate emulsion in aqueous phase aiding in oil recovery during LSWF for sandstones. Shaik et al. (2022) coated straight channel glass micromodels with $CaCO_3$ to transform the internal glass surfaces to carbonate using the layer-by-layer deposition method. The calcite-coated micromodel was used to investigate the effect of brine composition (e.g., salinity and ionic strength) in altering the wettability of calcite surfaces.

Solid-fluid physiochemical interaction is another area proven to be advantageous studying with geomaterial micromodels. Porter et al. (2015) investigated the advantages of using real rock micromodels to study the fracture-matrix interactions at a temperature and pressure consistent with the reservoir conditions. They developed a micromodel fabrication method that works well for both real rock and synthetic (e.g., glass, PDMS) micromodels.

Oh et al. (2017) investigated the interactions of a synthetic $PbCl_2$ solution and Uranium (U) containing groundwater with shale and granite surfaces using the micromodels they developed by placing thin sections of the respective rocks in a PDMS micromodel. While studying the

sorption of Pb and U onto the thin section, they stated that microfluidic tests are capable of mimicking mineral-fluid interactions in porous media, and micro X-ray fluorescence (μ-XRF) can be coupled with the microfluidic system to analyze the mineral surface after the interactions with fluid.

Siadatifar et al. (2021) prepared sandstone and carbonate representing geomaterials to visualize the fluid-fluid and solid-fluid interaction during LSWF. Jahanbakhsh et al. (2020), while reviewing the advancement in the fabrication method of micromodels and imaging techniques, reported that materials used for micromodel preparation could not fully capture the subsurface rock-fluid interactions. Hence, they emphasized functionalizing micromodel surfaces with geomaterials to replicate the surface mineralogy and wettability of the porous medium.

Two different methods have been used so far to functionalize the traditional glass or PDMS micromodels with clay minerals: physical adsorption by flowing clay slurry through the flow network (Amirian et al., 2017; Song and Kovscek, 2015) and a layer by layer deposition of polyelectrolyte and clay (Pan et al., 2019; Zhang et al., 2018). Song and Kovscek (2015, 2016) functionalized a silicon microfluidic chip with Kaolinite clay by injecting a clay solution of 1 wt.% of Kaolinite in 15,000 ppm brine to understand the effect of low salinity water flooding in sandstone reservoirs. After coating, to create an immobile clay surface and study the wettability alteration due to clay adsorption, they heat treated the surface at 120 ^{o}C for 25 minutes. A similar approach was adopted by Amirian et al.(2017) to develop Kaolinite (Amirian et al., 2017) and by Amirian and Haghighi (2018) to develop Illite coated geomaterial surfaces to understand the effect of clay type and water composition on low salinity water flooding. They used a 20 wt.% of clay slurry in 30,000 ppm NaCl brine, and instead of heat drying the coated surface, they air-

dried it for two hours by placing it on a hot plate set at 80 °C to ensure the reversibility of the coating.

Barnaji et al. (2016), instead of using any brine for base fluid, used a suspension of 10 wt.% of clay in distilled water to coat glass micromodels with Kaolinite and Na-Bentonite clays and dried the micromodels by placing them in an oven at 120 °C for 1 hour. Na-Bentonite was also used by Sharifipour et al. (2019) to coat glass micromodels and study pore-scale swelling behavior of the clay. For the coating purposes, they prepared two different clay slurries: one with 45000 ppm NaCl and 11800 ppm $CaCl_2$, and the other one with 1000 ppm NaCl. Following the coating, they heated the micromodels at 150 °C for water evaporation.

Mehdizad et al. (2022) etched the heterogeneous pattern of a real sandstone rock on the glass micromodel to represent the physical rock network of sandstone and then coated it with Na-Bentonite clay to study the recovery mechanisms in water-wet and oil-wet clay-rich heterogeneous micromodels. 5 wt.% clay slurries prepared with 57000 ppm NaCl brine were injected into the micromodel. During injection, the micromodel was placed in an ultrasonic bath to avoid clay flocculation and ensure homogenous deposition. The clay-saturated micromodel was then heated to 140 °C for water evaporation.

Shahmohammadi et al. (2021), to study the interactions between crude oil, brine, and clay, developed Montmorrilonite coated micromodels. To fabricate the micromodel, they first laser engraved a graphic pattern onto a glass plate. Afterward, a new glass plate was fused with the engraved one at a temperature of 710 °C to create the flow channel. A 41,600 ppm brine containing components such as NaCl, KCL, $MgCl_2.6H_2O$, $CaCl_2.2H_2O$, Na_2SO_4, $NaHCO_3$ at varying concentrations was used as the base fluid for the clay slurry. The slurry was prepared by

dissolving 60g of Montmorillonite clay in one liter of brine. Following the coating, they heat-treated the micromodel at a temperature of 120 ^{o}C for 1 hour.

Bartels et al. (2017) employed a new deposition method to prepare clay-coated glass micromodels. Instead of using brine to prepare the clay slurry, they used Isopropyl Alcohol (IPA). 60g of Montmorillonite clay was mixed with per liter of IPA to prepare the suspension. IPA was chosen to facilitate rapid drying of the micromodel. The drying was achieved by placing the clay-saturated micromodel in a vacuum oven at 60 ^{o}C. Their slurry preparation method was derived from the method developed by Mahani et al.(2015), who used deionized water to prepare the Na-Montmorillonite clay suspensions. The suspensions had a varying range (100-500 mg/L) of clay concentration. Following the coating, they vacuum dried the glass slide in desiccators for 5 to 10 minutes.

The use of deionized water in preparing the clay slurry is also prevalent in the work of Lebedeva and Fogden (2010). They coated a flat glass substrate with Kaolinite clay to investigate the adhesion of oil to Kaolinite. The slurry was prepared by dissolving 10g of Kaolinite clay in 50g of deionized water. The solution was heated at 85 ^{o}C until the final concentration reached 7 wt. %. Immediately after the glass slides were coated with clay, the substrate was swept by a heat gun at 120 ^{o}C to immobilize the clay particles.

A similar approach was taken by Bondino et al. (2013) and Kashiri et al. (2021) to prepare Kaolinite coated glass micromodel and study the effect of clay on oil recovery and fines migration during low salinity water flooding. While the former prepared a 0.31 wt.% of clay solution in deionized water and dried the coated substrate in an oven at 80 ^{o}C for three days followed by heating with a heat gun for 1 minute, the latter used 5 wt. % of clay solution and air-dried the substrate at 80 ^{o}C for 2 hours to prevent irreversible clay coating. Table 1 summarizes

235 the specifications of the clay slurries and the drying treatments employed by the researchers
236 mentioned in this study to prepare the clay-coated micromodels.

237

238 *Table 1: Summary of selected studies on preparing clay-coated micromodels*

Reference	Clay mineral	Clay concentration	Base fluid	Drying temperature	Drying duration
Song and Kovscek (2015, 2016)	Kaolinite	1 wt. %	15,000 ppm NaCl brine	120 °C	25 minutes
Amirian and Haghighi (2018); Amirian et al. (2017)	Kaolinite, Illite	20 wt. %	30,000 ppm NaCl brine	80 °C	2 hours
Barnaji et al. (2016)	Kaolinite, Na-Bentonite	10 wt.%	distilled water	120 °C	1 hour
Sharifipour et al. (2019)	Na-Bentonite	Not reported	45,000 ppm NaCl and 11,800 ppm $CaCl_2$; 1000 ppm NaCl	150 °C	Not reported
Mehdizad et al. (2022)	Na-Bentonite	5 wt.%	57,000 ppm NaCl brine	140 °C	Not reported
Shahmohammadi et al. (2021)	Montmor-illonite	6 wt. %	41,600 ppm brine containing NaCl, KCL, $MgCl_2.6H_2O$, $CaCl_2.2H_2O$, Na_2SO_4, $NaHCO_3$	120 °C	1 hour
Bartels et al.(2017)	Montmorillonite	6 wt.%	IPA	60 °C	Not reported
Mahani et al. (2015)	Na-Bentonite	100-500 mg/L	Deionized water	Not reported	5 to 10 minutes

Lebedeva and Fogden (2010)	Kaolinite	7 wt. %	Deionized water	120 °C	Not reported
Bondino et al. (2013)	Kaolinite	0.31 wt.%	Deionized water	80 °C	3 days +1 minute
Kashiri et al. (2021)	Kaolinite	5 wt. %	Deionized water	80 °C	2 hours

239

240 As it can be seen, there is not a good agreement between the works of literature on the
241 specification (e.g., salinity) of base fluid used to make the clay suspension. The post-coating
242 treatments (e.g., the temperature and duration of drying) also vary widely in the literature.
243 However, as per the DLVO theory, the presence or absence of cations in the carrier fluid is
244 critical for the attachment or detachment of clay particles from the rock surface as it controls the
245 colloidal forces acting between the particles and the solid surface (Berg et al., 2010; Schembre et
246 al., 2006). The temperature and duration of drying are also equally important to achieve
247 sufficient stability of the coating. For a successful preparation of the geomaterial model, the heat
248 treatment should not make the clay particles completely immobile. Having a stable coating
249 without compromising the natural mobility of the clay particles will make the geomaterial
250 surface a close representative of the clay-rich rock surface. Given the rise in the application of
251 clay-coated geomaterial surfaces, it is therefore imperative to evaluate the effect of base fluid's
252 salinity on clay adsorption and post-coating treatment on the stability of the coated surface to
253 reach a consensus over the solution preparation and drying procedures for a stable clay coating.

254 In this study, glass capillary tubes are coated with Illite clay slurries made with brines of four
255 different salinities to investigate the effect of salinity on clay adsorption to the glass surface. The
256 best performing clay-brine combination is then used to coat straight channel resealable
257 borosilicate glass micromodels. Once a uniform coating is obtained, the micromodels are dried at

different temperatures. The treated surfaces are then exposed to brines of different salinities to assess the effect of heat treatment on the stability of the adsorbed clay particles.

In the following sections, the method used for clay coating on a glass surface that includes several cycles of continuous injection and withdrawal of clay solution is described. Scanning electron microscopy (SEM) and Energy-dispersive X-ray spectroscopy (EDS) data of the clay-coated surfaces after each experiment are used to demonstrate the clay coating density, coverage, and chemistry. The effect of heat treatment on the stability of the coated surfaces is also discussed.

Experiments with brines of different salinities as the base fluid for clay slurry indicated a strong relationship between the brine's salinity and clay particles' adsorption on the glass surface. An increase in brine concentration resulted in improved adsorption of Illite clay particles on the glass surface. Experiments involving heat treating the coated glass surfaces also demonstrated a significant effect of temperature on the coating stability.

3 Materials and methods

3.1 Clay minerals

Illite (IMt-1) from Silver Hill's Cambrian Shales, Jefferson Canyon, Montana, USA, obtained from the source clays repository of the Clay Minerals Society was used to coat the glass capillary tubes. Prior to coating, the clay chips were powdered in a ball mill for less than five minutes. To avoid trace contamination of Fe or Al, a Tungsten canister and balls were used to grind the clay chips. To coat the straight channel glass micromodels, Illite clay powder (IMC) was purchased from Lotioncrafter.

279 Illite, $(K, H_3O)(Al, Mg, Fe)_2(Si, Al)_4O_{10}[(OH)_2, H_2O]$, is a 2:1 clay mineral where one octahedral
280 Alumina sheet is sandwiched between two tetrahedral Silica sheets. They have potassium ions
281 between each Tetrahedral-Octahedral-Tetrahedral (TOT) sequence making them less vulnerable
282 to water encroachment. The Illite IMt-1 sample had already been characterized by Köster (1996).
283 He identified the chemical composition of the clay sample by X-Ray diffraction analysis of
284 various size fractions of the clay sample (Köster, 1996) . Table 2 shows the elemental
285 compositional result obtained from the EDS elemental analysis of the Illite powders.

286 Table 2: Major components of the Illite clay (IMt-1 and IMC) as observed in EDS elemental map

	Mass Norm. %	
Element	**IMt-1**	**IMC**
Oxygen	46.50	51.80
Silicon	23.00	12.38
Aluminum	14.62	7.73
Potassium	7.80	2.60
Iron	5.23	3.14
Magnesium	1.58	1.50
Calcium	0.72	20.36
Titanium	0.37	0.34
Sodium	0.06	0.17
Zinc	0.03	0.01
Phosphorus	0.02	0

287

288 Clay minerals usually possess two different charges, one on the basal faces that arises from the
289 isomorphic substitution in the structural layers and exhibits permanent negative charges. The
290 other one is called the edge charge resulting from the protonation or deprotonation of the Si-OH
291 group depending on the pH and the ionic strength of the solution (Środoń, 1999). However, Illite
292 is less complicated in charge heterogeneity than Kaolinite and Smectite. The permanent negative
293 charge in the faces of Illite clay owing to the isomorphic substitution, is mostly balanced by the

interlayer potassium ion and thus does not contribute much to the electrostatic interaction between clay particles and the glass surface (Kumari and Mohan, 2021).

Nevertheless, in this study, instead of the surface charge of basal planes or edges, the net surface charge of Illite clay particles is used to explain the electrostatic interaction between the clay particles and the glass surface. In the alkaline pH condition and salinity range (0 to 30,000 ppm NaCl) of the clay solutions used in this study, the net surface charge of Illite is negative (Shehata and Nasr-El-Din, 2015).

3.2 Test Fluids

Clay slurries prepared with NaCl brines of different concentrations are specified in table 3. The brines were prepared by dissolving NaCl powder purchased from Sigma Aldrich in deionized water (18.2 MΩ-cm).

Table 3: Basic properties of the clay solutions

Illite clay slurry	Base fluid	NaCl concentration, ppm	Dynamic viscosity of clay slurry, cP	Density of clay slurry, g/cm^3	pH of clay slurry
01	DI water	0	0.5	1.5	8
02	Brine 1	5000	1.1	1.6	8.5
03	Brine 2	10000	1.2	1.65	8
04	Brine 3	30000	1.5	1.75	8.4

3.3 Solid substrates

Two different glass substrates were used for the coating purpose: capillary tubes and straight channel resealable flow cells. Glass capillary tubes purchased from DWK Life Sciences Kimble (catalog no. 34505–99) were used to develop the coating procedure and study the effect of base fluid's salinity on the adsorption of clay particles to the glass surface. The capillary tubes are

made of borosilicate glass, 90 mm long, and have an outer diameter of 1.2-1.5 mm and a wall thickness of 0.2 mm.

Straight channel resealable flow cells, purchased from Micronit Micro Technologies B.V, were used to prepare the geomaterial surfaces and study the effect of heat treatment on the stability of the clay coating (Fig. 1). Flow cells are composed of two separate layers. The bottom layer is a 700 µm thick plain glass slide, whereas the top layer is a 1100 µm thick glass slide with inlet and outlet ports enclosed by an elastomer. When the bottom and top layers are installed in the chip holder, the elastomer seals the top and bottom layer and defines the flow path. The flow path is about 40 mm long and has a hydraulic radius of 1.5 mm. One of the major advantages of these flow cells is that they are resealable, meaning that the top and bottom layer can be separated, and the surface can directly be used for microscopic analysis. Unlike the traditional microfluidic chips, those specially designed resealable flow cells do not have any flow network etched on them as the elastomer defines the flow path. Since no etching was involved, we believe the glass surfaces are molecularly smooth.

Moreover, for all the experiments same surfaces were used, i.e., surface roughness was not a varying parameter among the experiments. The only parameter that has been changed is the salinity of the clay solution so that any improvement in the clay coating can primarily be attributed to the base fluid salinity. Before coating, the substrates were treated with Nitrogen plasma to remove any organic contamination from the surface and improve the hydrophilicity (Shaik et al., 2020).

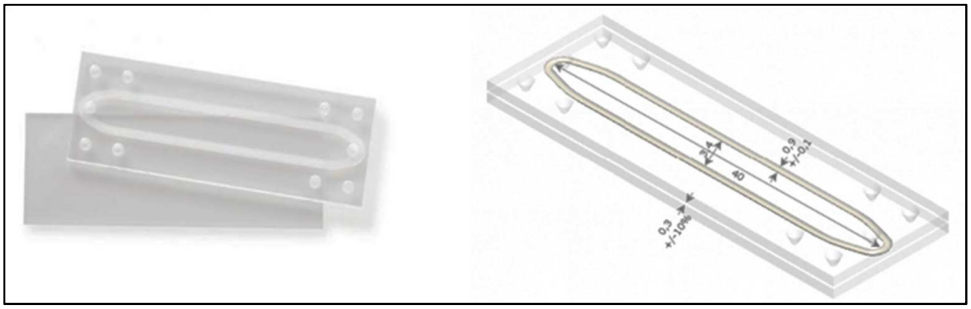

Figure 1: (left) Top and bottom part of resealable straight channel flow cell; (right) connected flow path with dimensions (Courtesy: Micronit Microfluidics).

3.4 Experimental procedure

3.4.1 Solution preparation

10 wt.% Illite clay slurries prepared in NaCl brines of different salinities were used to coat the glass capillary tubes and the resealable glass micromodels. The concentration of clay was selected based on several trial experiments to avoid the clogging of the channels and have sufficient clay particles to be adsorbed on the surface. The primary reason for using NaCl brine as the base fluid is to represent the subsurface reservoir environment and prevent in situ fines migration and clay swelling caused by freshwater interaction with clay.

Slurries prepared with brines of four different salinities were used to evaluate the effect of salinity on clay adsorption to the glass surface. The properties of the brines are listed in table 4. As the brine salinity increases, the clay particles are more prone to aggregating and settling down due to the decrease in the double layer repulsive forces. Therefore, to keep the particles dispersed in the solution, the clay slurries were vigorously stirred with a magnetic stirrer for 30 minutes, followed by ultrasonication using Branson 2800 Ultrasonic Cleaner for 1 hour and immediately injected into the capillary tubes.

Table 4: Specifications of the brines used to study the stability of the coating after each heat treatment

Brine concentration, ppm	Dynamic viscosity at 25°C, cP	Surface tension, N/m	Capillary number	Flow rate, µL/min	Micromodel volume, µL	Pore volumes injected
30000	0.948	0.072	1×10^{-6}	32.19	300	37.73
10000	0.909	0.072	1×10^{-6}	33.58	300	39.39
5000	0.893	0.072	1×10^{-6}	34.18	300	40.11
0	0.892	0.072	1×10^{-6}	34.22	300	40.16

3.4.2 Clay coating

There have been mainly two mechanisms behind glass surface getting coated with geomaterials: physical adsorption (Amirian et al., 2017; Song and Kovscek, 2015) and a layer by layer deposition of the minerals on the substrate surface (Shaik et al., 2020; Zhang et al., 2018). In the former method, the mineral slurry is flowed through the substrate surface, while in the latter case, a polyelectrolyte is used to link between the solid substrate and the coating minerals. Because in the latter case the deposition is governed by electrostatic attraction between the glass surface, polyelectrolyte, and minerals, the coating is more stable than that can be achieved from mere physical adsorption. Despite this fact, in this study, the former method is used to develop the coated surface to achieve the following objectives: to avoid using any synthetic materials except the clay; to replicate the subsurface porous environment as much as possible; and to study the effect of salinity on physical adsorption to the glass surface. The coating procedure developed by Song et al. (2015) was used with a few modifications to improve the coating density and stability (Song and Kovscek, 2015).

Herein, a 10 wt.% clay slurry prepared in NaCl solution of 30,000 ppm is used to coat the glass capillary tubes. Since physical adsorption is driven by the Van der Waals attractive forces

between the glass surface and clay particles, 100 cycles of clay solution infusion and withdrawal were performed to increase the contact of clay particles with the glass surface. Each cycle was composed of three steps: infusion-delay-withdrawal. Fluids were infused at a velocity of 26.5 meters/hour and withdrew at 2.65 meters/hour using a Harvard Advanced Programmable Syringe Pump (PHD Ultra). A delay of 2 minutes between infusion and withdrawal was maintained to allow sufficient time for the clay particles to get adsorbed. Instead of infusing air through the tubes to displace the clay slurry after each injection, the clay slurry was withdrawn by creating a vacuum at the outlet to avoid air channeling inside the flow network and completely displace the clay slurry. The clay solutions were required to be ultrasonicated every ten cycles to keep the particles dispersed in the solution. The flow rates were selected based on several trial tests to deliver the clay slurry evenly into the flow volume and displace the fluid carrying unadsorbed and loosely attached particles without affecting the coating. The process flow diagram for Illite clay coating on glass capillary tubes is shown in figure 2. Following the coating, the capillary tubes were air-dried at 25 °C for 1 hour.

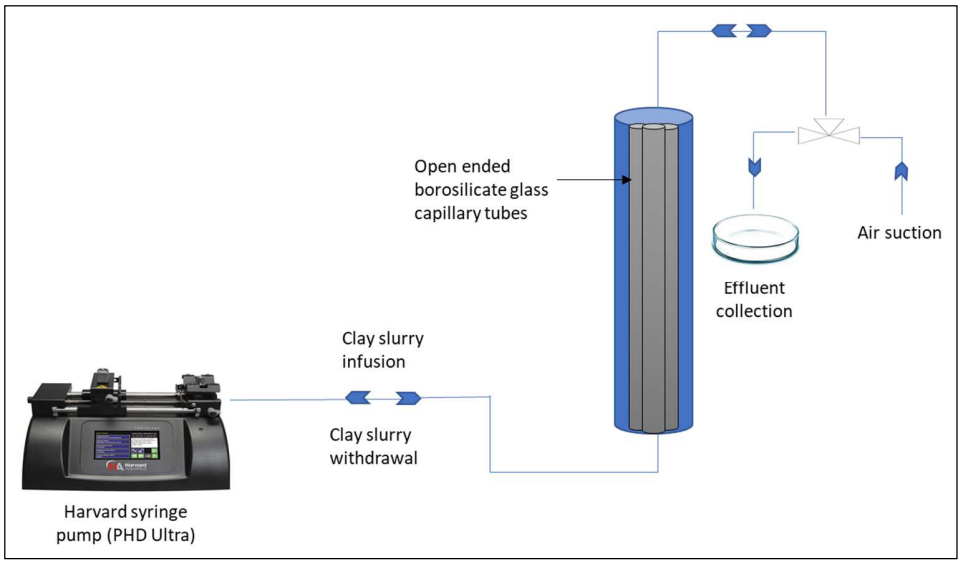

Figure 2: Process flow diagram for Illite clay coating on glass capillary tubes.

A very similar procedure was used to coat the resealable glass micromodels (Fig. 3). However, unlike the capillary tubes, the resealable flow cells had the facility to visualize the surface after each coating cycle, and only three cycles were observed to be sufficient to coat the glass surface uniformly; hence, the remaining cycles were not performed.

After drying, the capillary tubes were carefully broken into small pieces by gently pressing them with a tweezer to expose the coated surfaces for microscopic characterization. Coating coverage and uniformity were evaluated by AmScope 10X LED optical microscope, morphology by FEI Quanta 600 field-emission gun Environmental Scanning Electron Microscope (SEM), and elemental atomic percentages by Bruker Energy-Dispersive X-ray Spectroscope (SEM-EDS).

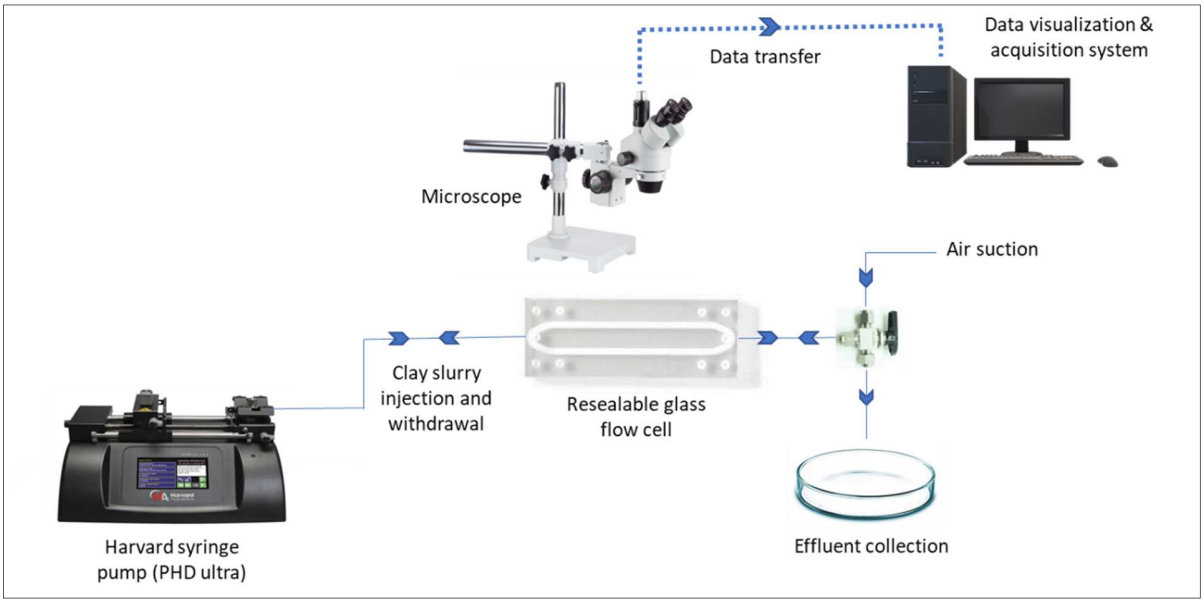

Figure 3: Process flow diagram for Illite clay coating on resealable glass micromodels

3.4.3 Evaluating effect of salinity

To evaluate the effect of base fluids salinity on the adsorption of Illite particles to the glass surface, four different clay slurries were prepared: three with NaCl brines of three different

399 salinities: 30,000 ppm, 10,000 ppm, and 5000 ppm and one with deionized water (DIW). The
400 deionized water represented the base fluid with no salinity. Following the coating, the surfaces
401 were air-dried at 25°C for one hour and afterward characterized with the bright-field optical
402 microscope, scanning electron microscope, and Energy-Dispersive X-ray Spectroscopy. The
403 optical images of the coated surfaces were analyzed with Fiji, a distribution of ImageJ software
404 to approximate the coating density.

405 **3.4.4 Heat treatment and coating stability analysis**

406 After the clay coating, the surface needs to be dried to make the particles adhered to it so as to
407 achieve the stability of the coating. For this purpose, the previous researchers have applied
408 different techniques that include heat drying the coated surface in an oven or with heat gun, air
409 drying, hot air drying at different temperatures, and for different time intervals (Amirian et al.,
410 2017; Bondino et al., 2013; Lebedeva and Fogden, 2010; Song and Kovscek, 2015).

411 In this study, the effect of heat treatment on the stability of the coating is evaluated. For this
412 purpose, straight channel resealable glass micromodels are coated with 10 wt.% Illite clay slurry
413 prepared in 30000 ppm NaCl solution. Two different post-coating treatments were used to dry
414 the coated micromodels. The first treatment involved drying the coated surface with air at room
415 temperature (25 °C) for 1 hour, while in the second method, the clay-coated surfaces were air-
416 dried gradually up to 125 °C for 25 minutes.

417 The release of clay particles from the clay-coated surface could be due to the instability of the
418 coating or the sensitivity of the clay particles to the fluid flowing on it. While the former one
419 depends on how firmly clay particles are attached to the substrate surface, the latter one is a
420 function of salinity or the number of counterions present in the fluid.

Prior to evaluating the stability of the coating, it is therefore, crucial to distinguish the release of clay particles owing to clay-brine interaction from that due to the instability of coating. Since the clay particles were already in contact with 30,000 ppm NaCl brine as the clay slurry was prepared with it, 30,000 ppm NaCl brine could be considered, in this case, as the formation water. Thus, the coating can be considered stable if the 30,000 ppm NaCl brine flooding for a sufficient period of time does not cause a significant release of clay particles from the glass surface. Any fluid having salinity less than this may cause the release of clay particles, and the effect is expected to increase as the salinity of the injection fluid gets decreased. Having said that, none of the fluids should completely remove the coating if the coating is indeed stable.

To evaluate the sensitivity of the coated surface to the fluid flowing on it, the micromodels were exposed to flooding of base brine (30000 ppm) and the brine of reduced salinity (10,000 ppm) and DI water for six hours. After each flooding, vacuum suction was employed to take away loosely attached clay particles and brine. The fluid flow was conducted at the rates specified in Table 4. These flow rates were chosen to maintain a low capillary number (1×10^{-6}) so that the release of clay particles during the flow is driven by clay-fluid interaction, not by viscous force. Afterward, the surfaces were dried in the oven at 100 °C for 30 minutes to get away with any water left on the glass surface.

3.4.5 Microscopic characterization of coating stability

Following oven-drying, the brine exposed resealable chips were disintegrated. Then, the bottom wall was evaluated with optical and SEM microscopy to observe the coating state after each flooding. It should be noted that the bottom wall of the flow cell had a slightly higher coating density than the top one, hence used for the microscopic analysis. This might be due to the effect

443 of gravity that led to the increased deposition of clay particles on the bottom wall. This
444 observation was consistent with the findings of Zhang et al. (2019) [49].

445 Confocal laser scanning microscopy was used to develop 3D reconstructed images of the mineral
446 coatings on the glass surface following each stability test. The surfaces were excited with 488 nm
447 laser lines, and no fluorescent dyes were added to the samples as the clay particles were auto-
448 fluorescent. Each of the surfaces was divided into a number of slices based on the focus planes,
449 and 2D images taken under the bright-field mode from each of the slices were stacked together to
450 make 3-D reconstructed images of the optical section of the sample. The 3D images provided
451 insights into the effectiveness of heat treatment on the stability of the coating.

452 # 4 Results and discussions

453 ## 4.1 Functionalizing glass capillary tubes with Illite clay

454 Figure 4 shows bright-field microscopic images of the uncoated glass capillary tube surface and
455 the surface coated with 10 wt.% Illite clay slurry prepared in 30,000 ppm NaCl brine. With this
456 combination of the solution, a nearly uniform distribution of clay particles was observed on the
457 glass surface, indicating the efficacy of the developed coating procedure.

458 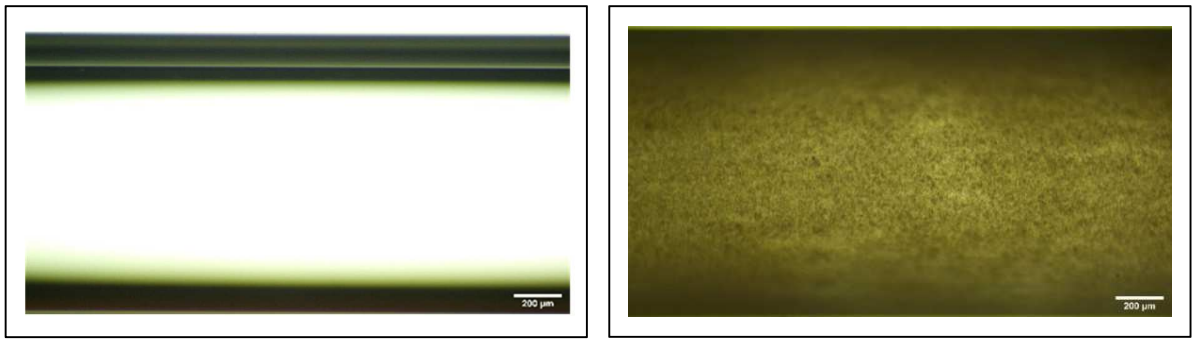

459 Figure 4: Microscopic image of the uncoated (left) and Illite-coated (right) glass capillary tube
460 surfaces.

461 Figure 5 shows the Scanning Electron Microscopic (SEM) image of the coated surface at
462 different magnifications. SEM-EDS elemental map of the coated surface is shown in figure 6.
463 Oxygen, Silicon, Aluminum, Potassium, Iron, and Magnesium were the major chemical elements
464 present in the Illite clay (IMt-1) used to coat the glass capillary tubes (Table 2). EDS elemental
465 map indicates the presence of those components on the coated surface as well.

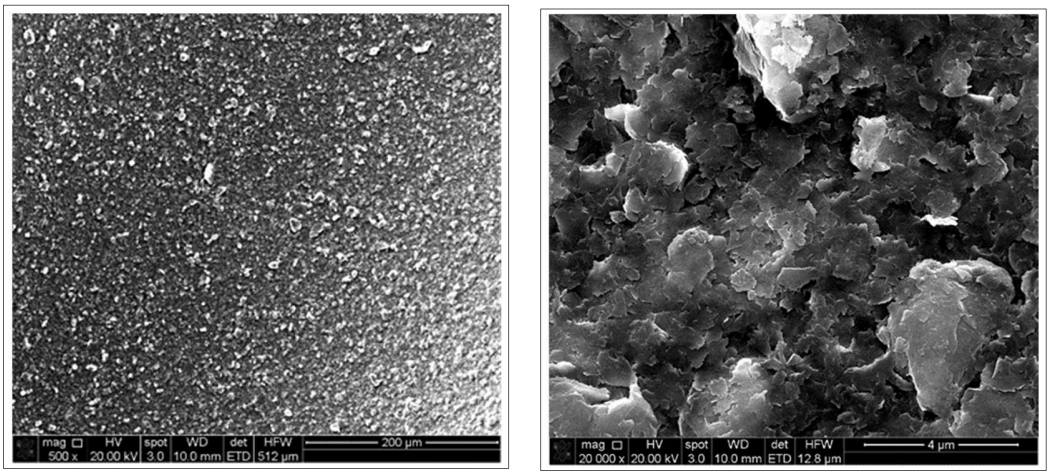

466
467 Figure 5: SEM image of the Illite-coated capillary tube surface at two different magnifications.

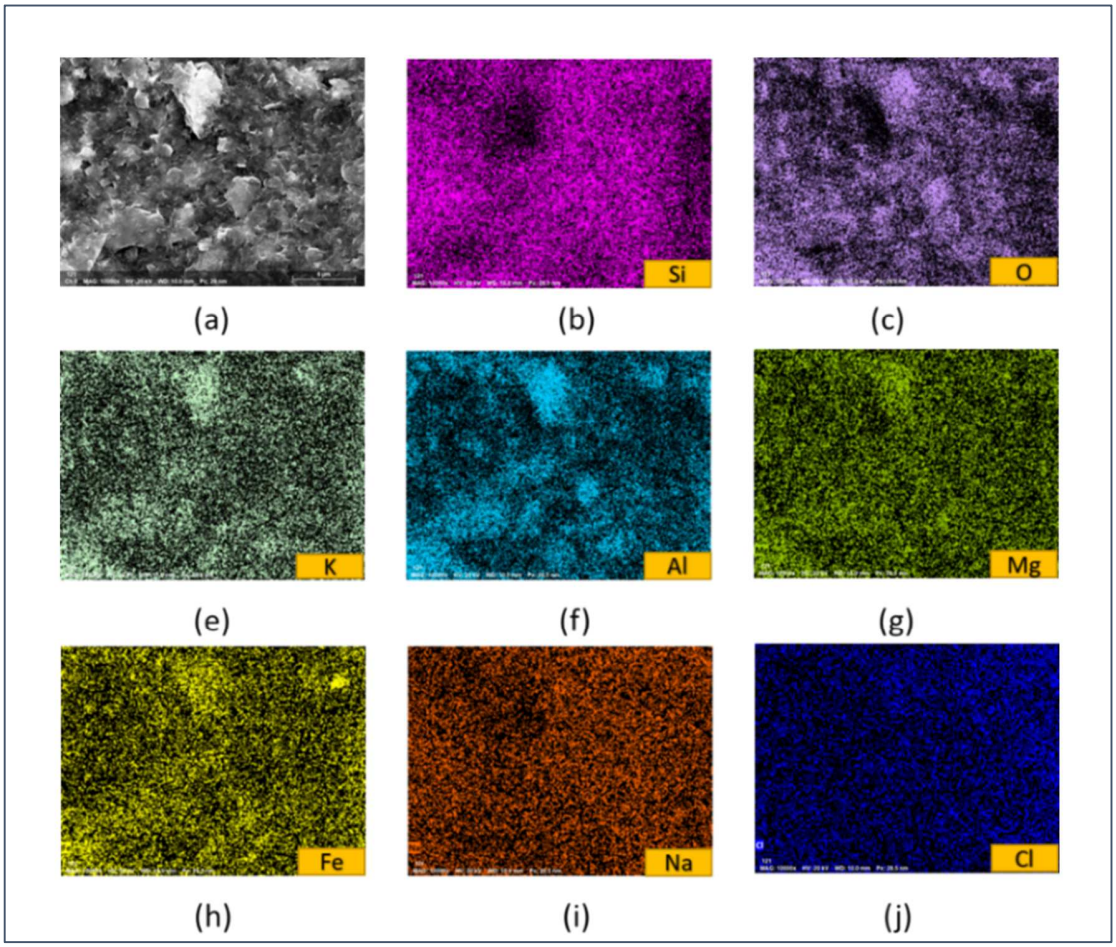

Figure 6: (a) SEM image and (b-j) EDS elemental map of the Illite coated glass capillary tube surface.

Table 5 shows the contribution of different components of the clay slurry on the coated surface as evidenced from the EDS elemental map. Even though, the clay slurry was prepared by dissolving Illite clay in high salinity NaCl brines, the marginal contribution of both Na and Cl on the elemental map indicates that only the clay particles were adsorbed on the glass surface.

Table 5: Contribution of different components of clay slurry on the coated surface as evidenced from EDS elemental analysis

Element	Mass, [%]	Mass Norm., [%]	Atom, [%]
Carbon	4.77	7.48	12.57
Oxygen	26.50	41.56	52.43
Sodium	0.72	1.13	0.99

Magnesium	0.56	0.87	0.73
Aluminium	5.30	8.31	6.22
Silicon	20.70	32.47	23.33
Chlorine	0.18	0.29	0.16
Potassium	2.96	4.64	2.40
Calcium	0.01	0.02	0.01
Iron	2.06	3.23	1.17
Total	63.75	100.00	100.00

478 **4.2 Effect of salinity on clay coating**

479 Glass capillary tubes coated with 10 wt.% illite clay prepared in NaCl solutions of four different
480 concentrations (0 ppm, 5000 ppm, 10000 ppm, and 30000 ppm) were created to evaluate the
481 effect of base fluids salinity on clay adsorption to the glass surface. Figure 7 shows the optical
482 microscopic images of the surfaces coated with those different clay slurries. It is observed that as
483 the brine concentration is increased, the coating coverage is improved. When the clay slurry is
484 created with DI water, there was seemingly no adsorption of the clay particles on the glass
485 surface. However, with higher concentrations of brine, the number of adsorbed particles
486 increased, and with 30000 ppm, a quasi-homogeneous coating is observed.

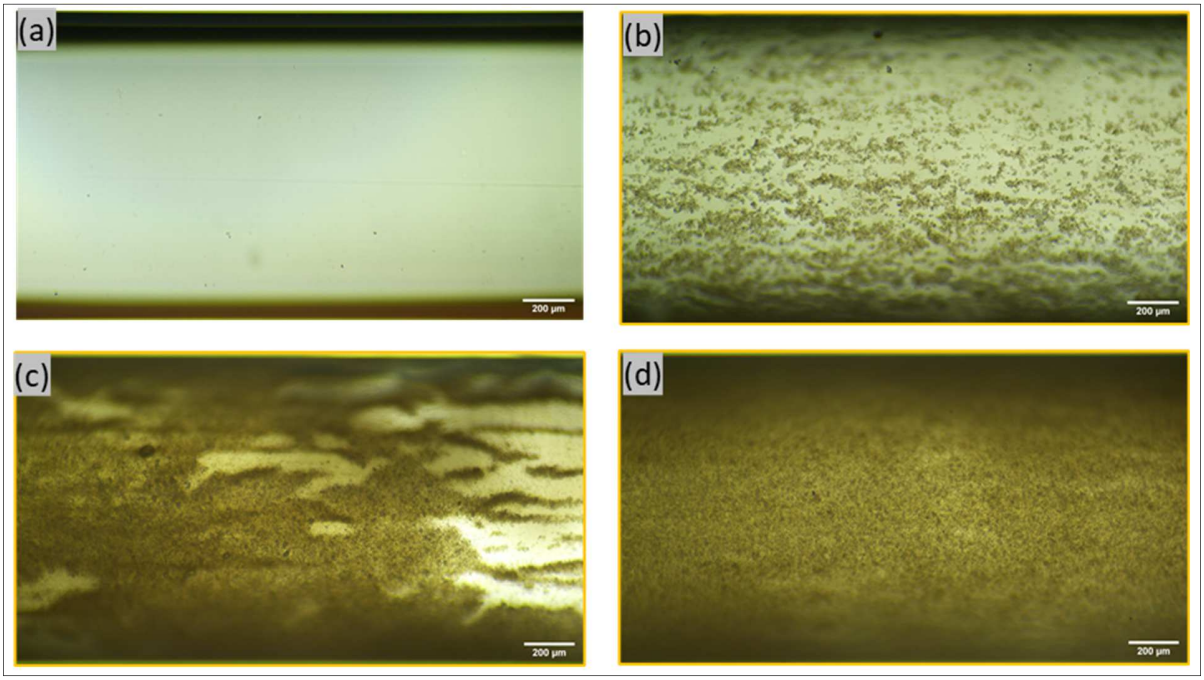

Figure 7: Glass capillary tubes coated with 10 wt.% Illite clay slurry prepared with: (a) DI water, (b) 5000 ppm NaCl, (c) 10000 ppm NaCl, and (d) 30000 ppm NaCl. Images are taken after drying the coated capillary tubes at 25 °C.

The coating density approximation (Fig. 8) revealed that, the coating coverage was around 49 % when the surface was coated with clay in 5000 ppm brine. When the surface was coated with clay in 10,000 ppm NaCl brine, the coating coverage increased to ~ 85 %. Finally, with 30,000 ppm NaCl, almost 98% coating coverage was obtained.

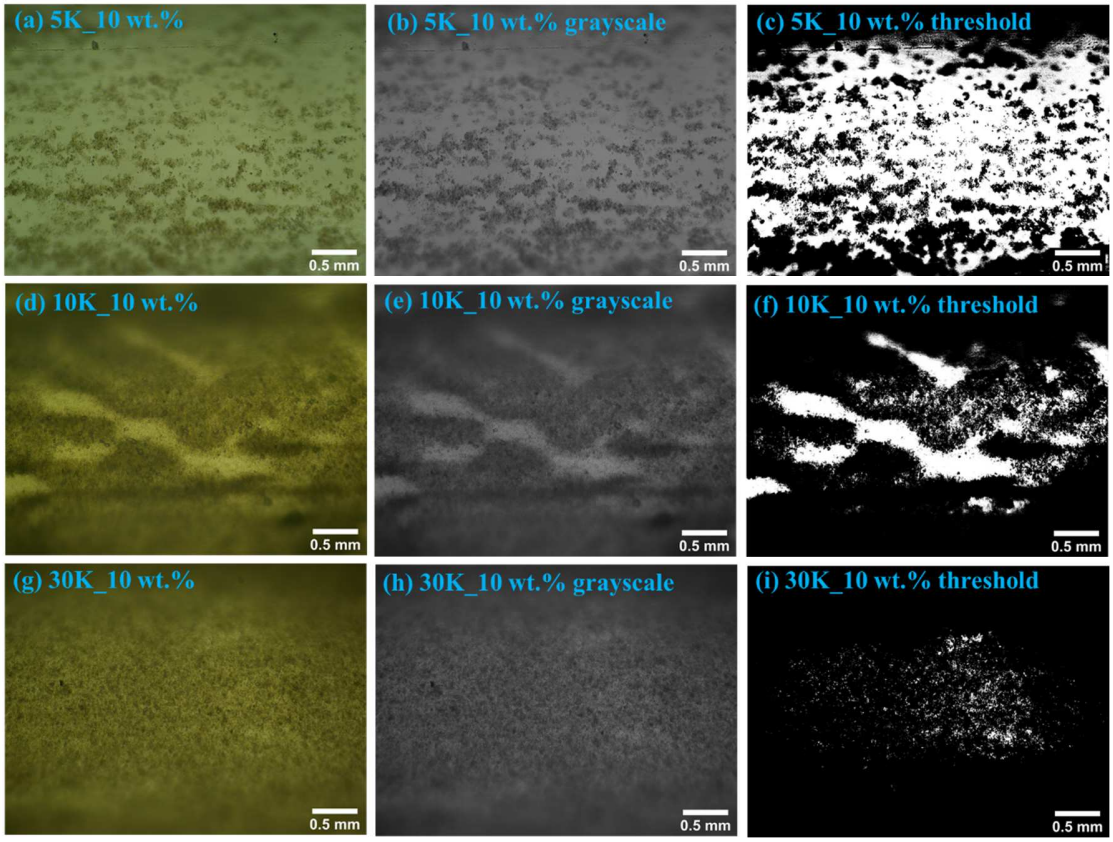

Figure 8: Coating density approximation with Fiji. High magnification (a, d, g) optical, (b, e, h) 8-bit grayscale, and (c, f, i) threshold images of the capillary tube surfaces after coating with clay slurry prepared in (a-c) 5000 ppm, (d-f) 10,000 ppm, and (g-i) 30,000 ppm NaCl brine. The rectangular region is showing the Region of Interest where the coating density is approximated.

EDS elemental map (Fig. 9) of the coated surface has also exhibited increased adsorption of clay particles on the glass surface when the slurry is prepared with the high salinity brine. Figure 9 (a) shows that the surface coated with clay slurry prepared in 5000 ppm brine has the elemental map dominated by the presence of silicon (Si). Even though Si is the primary constituent of both the solid substrate and the clay minerals, the significant dominance of silica here indicates the uncoated borosilicate glass surface as the primary source of it. Otherwise, there would also have a significant contribution of other clay components (e.g., Mg, Al, K, Ca, Fe, etc.) on the elemental map similar to figure 9 (b) and figure 9 (c). Increased concentration of brine (10,000 ppm and 30,000 ppm) resulted in increased adsorption of clay particles. As a result, the coated

surfaces display more distribution of other clay constituents besides Si on the EDS elemental map (Fig. 9 (b) and 9 (c)).

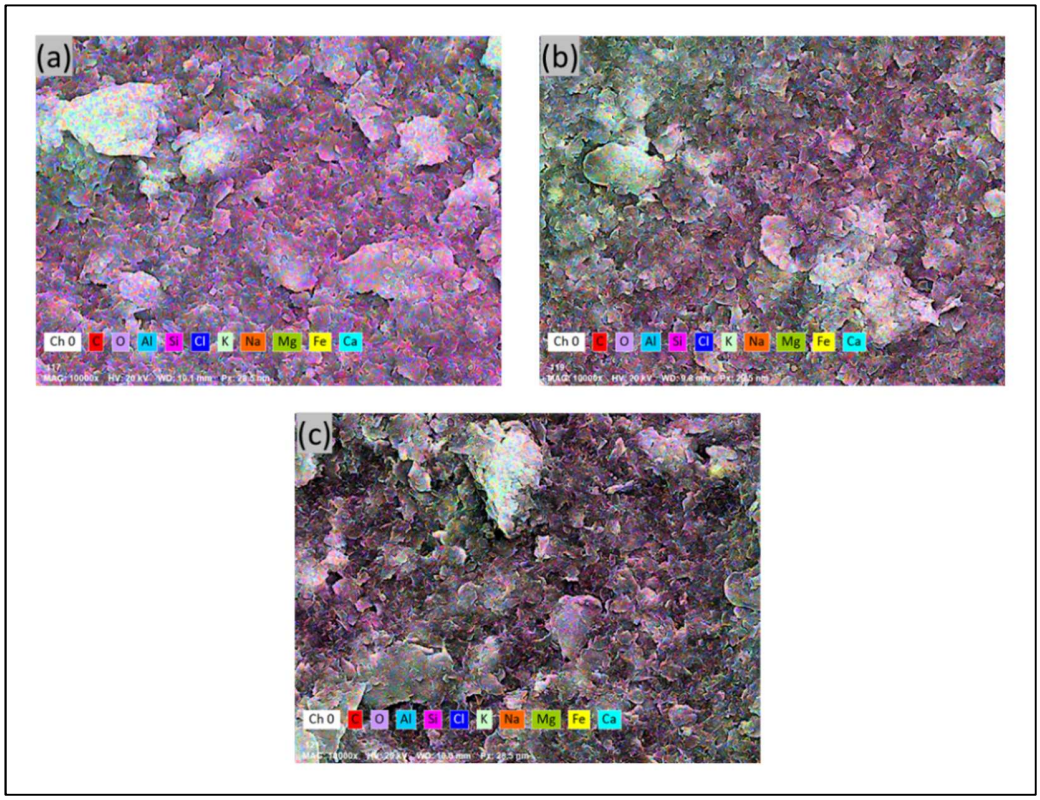

Figure 9: EDS elemental distribution maps of glass surfaces coated with Illite clay prepared in (a) 5000 ppm, (b) 10000 ppm, and (c) 30000 ppm NaCl solution. The color indexes are showing the presence of different chemical elements on the coated surface. Figure 9 (a) being dominated by purple color indicates less amount of clay adsorption on the glass surface, rendering the surface mostly uncoated. With the increased salinity of brine, a more balanced distribution of clay constituents is displayed in figure 9 (b) and figure 9 (c).

This effect of salinity on clay adsorption can be explained with the DLVO theory and attributed to the net effect of electric double layer (EDL) repulsive forces and Van der Waals attractive forces between the clay particles and the glass surface. It is well known that clay particles have a net negative surface charge, and glass surface, due to the dissolution of the silanol group, also exhibits a negative surface charge. However, the surface charge of the clay particles or glass surface might exhibit charge reversal from negative to positive at a high brine concentration or

524 even at a low concentration when the pH is in the acidic region due to the adsorption of H^+ ions
525 on the mineral surface. Since the pH of the clay slurries used in this study is not in the acidic
526 range (Tab. 3), the effect of the H^+ ion may not be applicable here. This leads us to the
527 possibility of charge reversal only due to the effect of high salinity brine.

528 However, for Illite clay particles and Quartz (the primary constituent of glass) to become
529 positively charged at the alkaline pH regions, the brine concentration must be higher than the
530 seawater (Shehata and Nasr-El-Din, 2015). At the alkaline pH region, the ζ-potential values of
531 Illite clay and Quartz in seawater (~38,000 ppm NaCl) are reported to be -5.3 mV and -2.5 mV,
532 respectively. The ζ-potential values get further decreased (increase in the negative value) as the
533 brines get diluted. The maximum brine concentration (30,000 ppm) used in our study is less than
534 the seawater salinity. Therefore, in the attempt to explain the effect of brines salinity on DLVO
535 forces, we assumed that the brine concentrations used in this study are not sufficiently high, and
536 the pH of the solution is not low enough to reverse the surface charge of either the clay particles
537 or the glass surface; hence both of the surfaces behave as negatively charged.

538 The development of a net negative charge on the clay particles' surface would cause an increased
539 concentration of counterions from the surrounding fluid in the interfacial region (electrical
540 double layer). However, in the case of clay solution prepared with deionized water or low
541 salinity brines, the lack of counterions causes expansion of the double layer (increase in Debye
542 Length). Therefore, double layer repulsive forces between the particles and glass surface
543 dominate over the effect of weak Van der Waals attractive forces between the particles and the
544 surface, hence not allowing the particles to get adsorbed on the glass surface.

As the brine concentration or the ionic strength of the clay solution increases, increased concentration of counterions from the surrounding fluid suppresses the thickness of the double layer (Debye Length). The extent of the repulsive forces also gets diminished.

In simpler words, as the ionic strength increases, the negative surface potential of the clay particles starts to get dropped off by the positive ions. Hence, the effect of electrostatic repulsive forces between the particles negates, and at a certain concentration of brine, Van der Waals attractive forces between the particles and the glass surface become the dominant force driving the adsorption of clay particles to the glass surface. The higher the effect of Van der Waals force, the better the adsorption would be. Therefore, we have seen an increase in the coating density with higher concentrations of brine, and at 30,000 ppm, a complete coverage of glass surface with clay particles was observed.

4.3 Preparing clay-coated micromodel

Figures 10 shows different states of the resealable microfluidic chip surface before and during the coating experiment. As can be deduced from the figures, the microfluidic chip was completely saturated with clay slurry and the vacuum suction of air from the chip outlet resulted in a very effective displacement of clay slurry and uniform distribution of adsorbed particles on the glass surface. Figure 11 shows the high magnification optical microscopic image of the Illite coated micromodel surface.

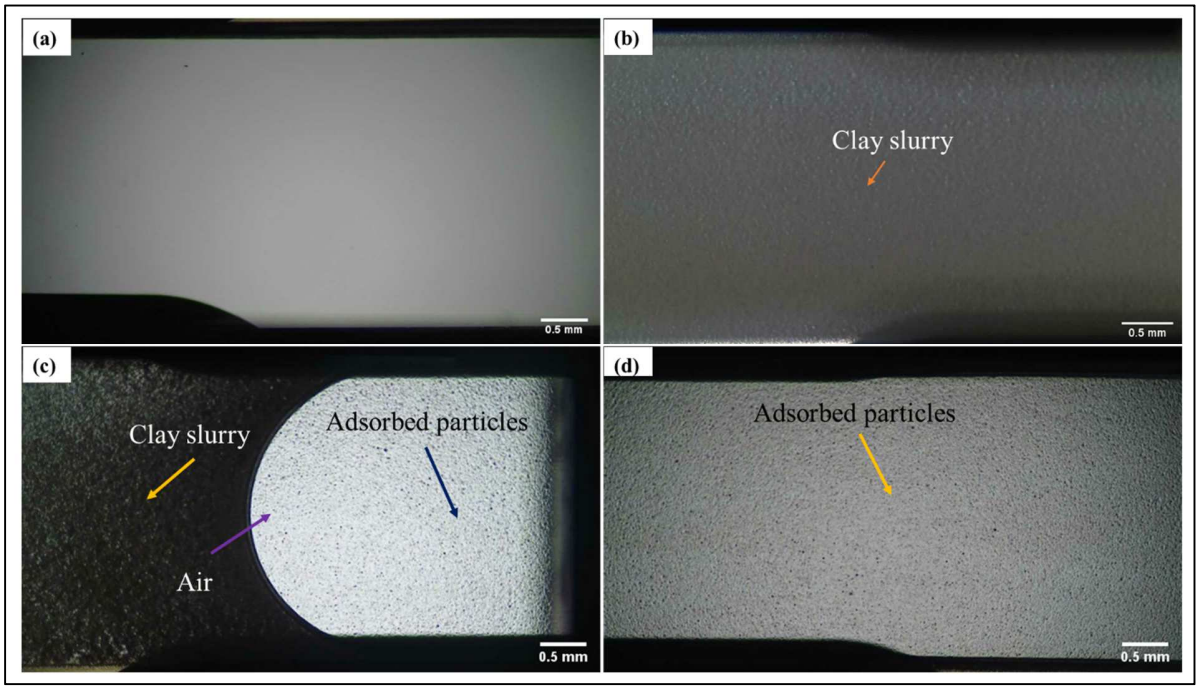

Figure 10: Micromodel surface at different states: (a) uncoated surface, (b) completely saturated with clay slurry after infusion, (c) vacuum suction leading to a uniform displacement of clay slurry, and (d) even distribution of adsorbed clay particles on the glass surface after complete withdrawn of the clay slurry.

Figure 11: High magnification image of the dried micromodel surface after Illite-clay coating.

4.4 Effect of heat treatment on coating stability

4.4.1 Stability characterization using optical microscopy

Figure 12 shows the optical microscopic images of the Illite coated surfaces after being exposed to brines of different concentrations and deionized water (diw) for 6 hours. Comparisons between figure 12 (a), 12 (b), and 12 (c) indicate that the surface dried at 125 °C has more similarity in coating appearance with the initial state than the one dried at 25 °C, where the release of clay particles is visually detectable. This implies that drying the clay-coated micromodel at 125 °C temperature improves the stability of the coating.

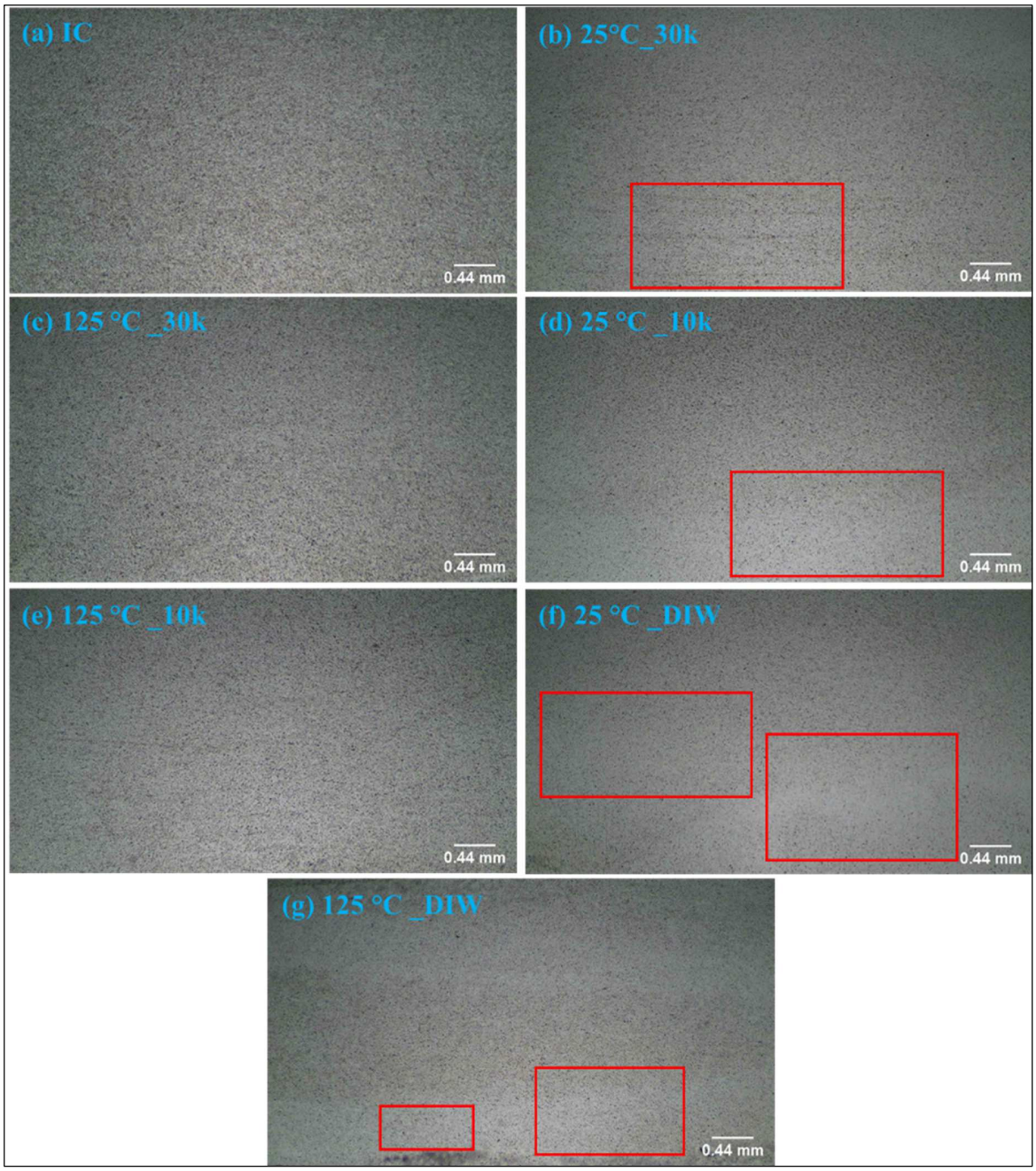

Figure 12: Optical microscopic images of the (a) initial state of the Illite-coated micromodel surface before flooding any fluid, state of the coated surface dried at (b) 25 °C and (c) 125 °C after exposed to 30,000 (30k) ppm NaCl brine, surface dried at (d) 25 °C and (e) 125 °C exposed to 10,000 (10k) ppm NaCl, and surface dried at (f) 25 °C and (g) 125 °C exposed to deionized water (DIW) for 6 hours during the dynamic flooding test. Red rectangles are showing some of the washout zones in the coated surface from where the clay particles are washed away or might have migrated to other locations as the surface came in contact with the liquids.

587 Figures 12 (d-g) reveal that, regardless of what temperature was used to dry the coated surface,
588 fluids with salinity less than 30,000 ppm brine caused detachment of the clay particles in both
589 types of surface. This implies that the heat treatment did not make the coating completely
590 immobile. However, the degree of sensitivity of the clay particles with the brines was affected by
591 the heat treatment. Compared to the Illite-coated surfaces dried at 25 °C, the surfaces treated at
592 125 °C temperature retained more particles attached to the surface following the flow of lower
593 salinity brines and deionized water.

4.4.2 Stability characterization using scanning electron microscopy

Similar to optical images, SEM images also exhibit a resemblance in the coating appearance between the initial condition (Figure 13 (a)) and the 125 °C treated surface exposed to 30,000 ppm brine flooding (Figure 13 (e)). However, unlike the optical image (Figure 12 (b)), SEM image of the 25 °C treated surface (Figure 13 (b)) shows a relatively denser coating than the initial state (Figure 13 (a)). This might be due to the very small field of view usually associated with SEM images and localized accumulation of clay particles being migrated from another location of the surface. Nevertheless, this also implies that the 25 °C treated surface was more prone to clay detachment than the one treated at 125 °C.

The effect of heat treatment is more evident in the SEM images of the coated surfaces exposed to low salinity brines (salinity < 30,000 ppm) and deionized water (Fig. 13 (c), 13 (d), 13 (f), and 13 (g)). Even though the release of particles is visible in both types of surfaces, the surface-treated at 25 °C was affected the most.

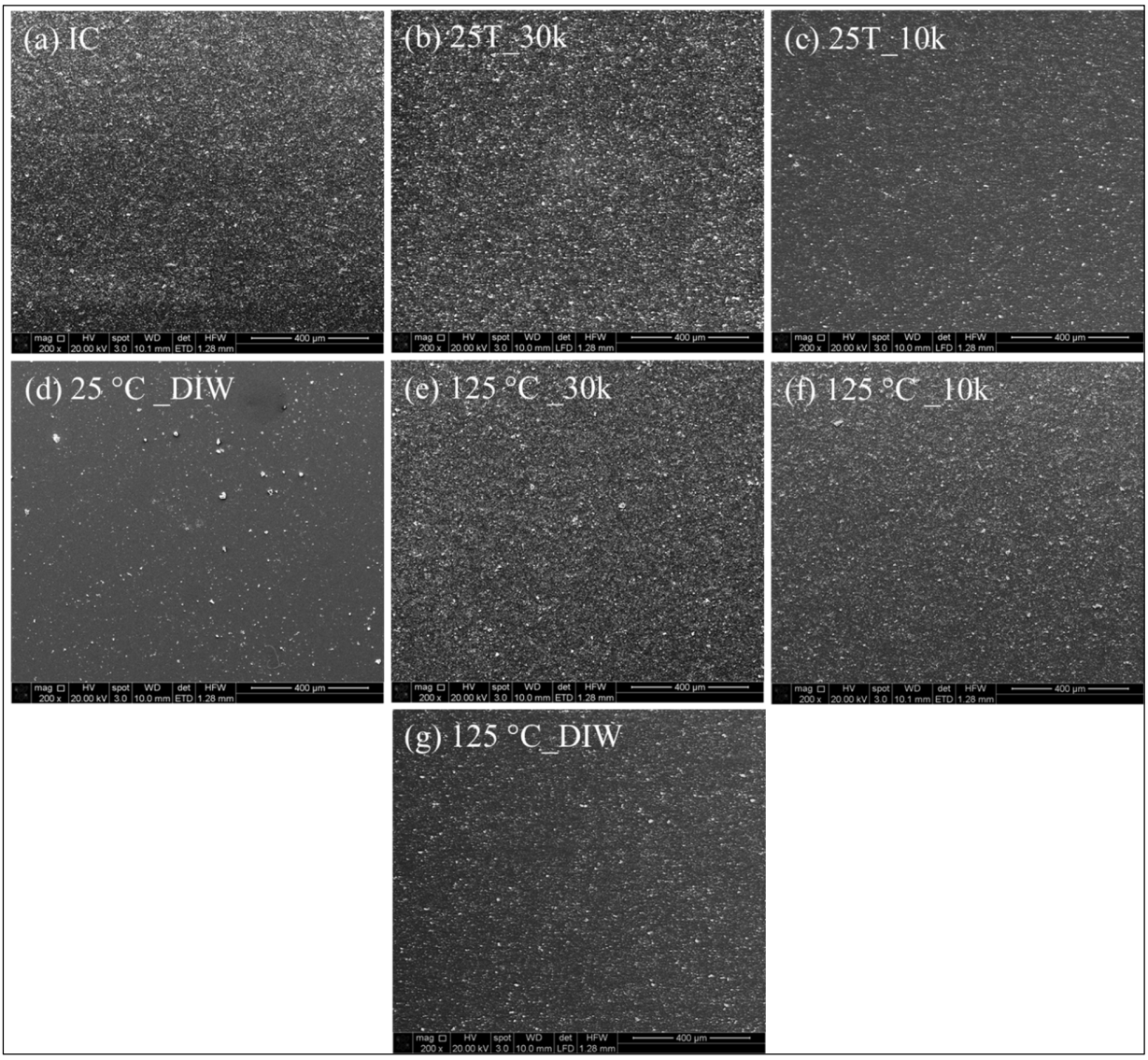

Figure 13: SEM images of the coated surfaces after exposed to brines of different concentrations for 6 hours. Figure 13 (a) shows the initial condition (IC) of the coated surface before flooding any fluid; (b) state of the coated surface dried at 25 °C after exposed to NaCl brines of 30,000 ppm (30K), (c) 10,000 ppm (10K), and (d) deionized water (DIW) for 6 hours; Figure 13 (e) shows the state of the coated surface dried at 125 °C after exposed to NaCl brines of 30K ppm, (f) 10K ppm, and (g) DIW for 6 hours.

4.4.3 Stability characterization using confocal laser scanning microscopy

Confocal laser scanning microscopy (CLSM) was used to further confirm the improved stability of the coated surface treated at 125 °C. Figure 14 shows the 3D reconstructed images of the coated surfaces after being exposed to 30,000 ppm NaCl brine and deionized water. The surfaces

were excited with 488 nm laser lines. No fluorescent dyes were applied to the auto-fluorescent clay minerals. Clay particles adsorbed the laser lights and caused the green fluorescence visible in figure 14.

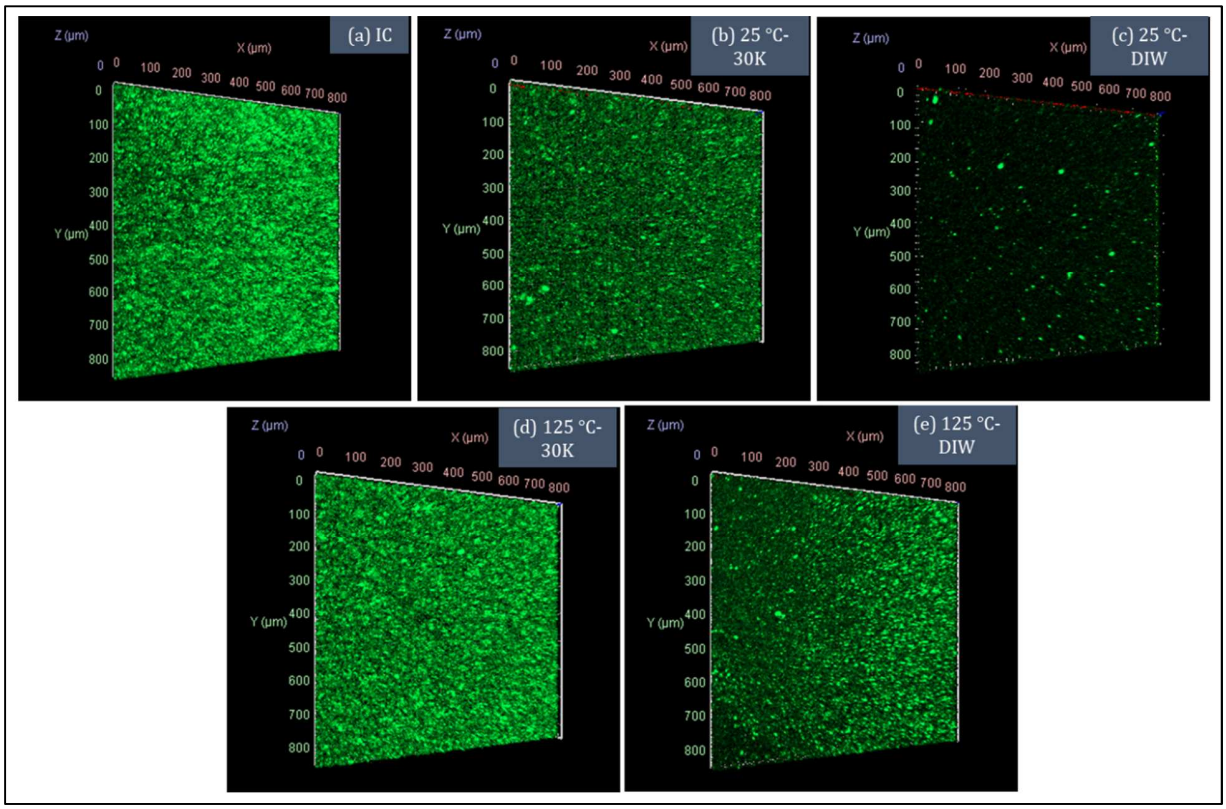

Figure 14: 3D reconstructed images of the mineral coatings over the glass surface showing the state of coating at different conditions. (a) The initial condition (IC)of the coated surface before flooding any fluid ; (b-c) state of the coated surface dried at 25 °C after being exposed to 30,000 ppm (30K) NaCl brine and deionized water (DIW) for 6 hours; (d-e) state of the coated surface dried at 125 °C after being exposed to 30,000 ppm NaCl brine and deionized water for 6 hours. Each image has the size of 848.53 µm × 848.53 µm × 40.5 µm.

Following the 30,000 ppm brine flooding, the surface treated at 125 °C exhibited more similarity in coating appearance with the initial state of the coating than the one treated at 25 °C. The surface dried at 25 °C and exposed to 30,000 ppm NaCl flow, displayed fewer green fluorescence when excited with the laser beams, indicates that a good number of clay particles have already been washed away from the surface.

The effect of heat treatment is more evident in the case of DI water flooding. Coating treated at 25 °C experienced wash away of most of the clay particles during the DI water flooding, as it can be deduced from the dearth of green fluorescence in Figure 14 (c). However, even though 125 °C treated surface also experienced some release of clay particles due to DI water flow, thus corroborating the fact that natural mobility of the clay particles was not compromised by the heat-treatment, the 125 °C treated surface had considerably more clay particles remained attached to the surface following the flooding compared tothe one treated at 25 °C. These observations are consistent with the findings from optical and SEM image analysis.

5 Conclusion

In this study, Illite-coated surfaces were successfully generated in borosilicate glass capillary tubes and resealable straight channel microfluidic chips made of borosilicate glass. It was observed that vacuum suction of air to displace clay slurry from the flow volume produced a very uniform and even distribution of clay particles on the glass surface. NaCl solution was used as the base fluid to prepare the clay slurry required to inject into the capillary tubes and microfluidic chip. The salinity of the NaCl solution was found to have a significant effect on the adsorption of clay particles to the glass surface. Based on the microscopic characterization and coating density approximation with Fiji, this study has shown that if the salinity or ionic concentration of the base fluid is increased, a more dense and uniform clay coating could be obtained on the glass surface. In this study, the slurry prepared with deionized water rendered no adsorption of clay particles on the surface, whereas with 30,000 ppm NaCl brine a more uniform and dense distribution of clay particles was observed.

655 The micromodel dried at 25 °C performed poorly even when contacted with the high salinity
656 brine. There were considerable detachments of the clay particles from the glass surface at
657 different locations. Deionized water caused the maximum damage as several wash-away zones
658 of the coated layer was seen in the optical, SEM, and CLSM images. In contrast, there were not
659 such detachments of the clay particles from the 25 °C treated glass surface when exposed to the
660 high salinity brine flooding for 6 hours. The temperature was enough to keep the particles firmly
661 attached to the surface without compromising the natural mobility of the clay particles. The
662 particles from a few locations got eventually detached when the surface came in contact with
663 lower salinity brine and deionized water.

664 ## 6 Acknowledgment

665 We acknowledge the financial support (Award Number: DE-FE0031776) from the U.S
666 Department of Energy (DOE) and Continental Resources Inc. We thank Dr. Jim Puckette for his
667 help in providing and preparing the clay samples. We also thank Mr. Sushobhan Pradhan and
668 Mr. Brent Johnson for their support during the microscopic analysis.

669 ## 7 References

670 Amirian, T. and Haghighi, M., 2018. Impact of clay type and water composition on low salinity
671 water injection–visualisation approach. The APPEA Journal, 58(1): 51-59.

672 Amirian, T., Haghighi, M. and Mostaghimi, P., 2017. Pore scale visualization of low salinity
673 water flooding as an enhanced oil recovery method. Energy & Fuels, 31(12): 13133-
674 13143.

675 Barnaji, M.J., Pourafshary, P. and Rasaie, M.R., 2016. Visual investigation of the effects of clay
676 minerals on enhancement of oil recovery by low salinity water flooding. Fuel, 184: 826-
677 835.

678 Bartels, W.-B. et al., 2017. Oil configuration under high-salinity and low-salinity conditions at
679 pore scale: a parametric investigation by use of a single-channel micromodel. SPE
680 Journal, 22(05): 1,362-1,373.

Berg, S., Cense, A.W., Jansen, E. and Bakker, K., 2010. Direct experimental evidence of wettability modification by low salinity. Petrophysics - The SPWLA Journal of Formation Evaluation and Reservoir Description, 51(05).

Bondino, I., Doorwar, S., Ellouz, R. and Hamon, G., 2013. Visual microscopic investigations about the role of pH, salinity and clay on oil adhesion and recovery, International Symposium of the Society of Core Analysts held in Napa Valley, California, pp. 16-19.

Campbell, B.T. and Orr, F.M., 1985. Flow visualization for CO_2/crude-oil displacements. Society of Petroleum Engineers Journal, 25(05): 665-678.

Cihan, A. et al., 2022. Permeability Decline by Clay Fines Migration around a Low-Salinity Fluid Injection Well. Groundwater, 60(1): 87-98.

Fang, W. et al., 2017. Investigation of salt and alkali sensitivity damage mechanisms in clay-containing reservoirs using nuclear magnetic resonance. Particulate Science and Technology, 35(5): 533-540.

Gaol, C.L., Ganzer, L., Mukherjee, S. and Alkan, H., 2021. Parameters govern microbial enhanced oil recovery (MEOR) performance in real-structure micromodels. Journal of Petroleum Science and Engineering, 205: 108814.

Ghazanfari, M.H., Rashtchian, D., Kharrat, R. and Vossoughi, S., 2007. Capillary pressure estimation using statistical pore size functions. Chemical Engineering & Technology: Industrial Chemistry-Plant Equipment-Process Engineering-Biotechnology, 30(7): 862-869.

Gomez, S.L. and He, W., 2012. Fighting wellbore instability: customizing drilling fluids based on laboratory studies of shale-fluid interactions, IADC/SPE Asia Pacific Drilling Technology Conference and Exhibition. Society of Petroleum Engineers.

Grattoni, C.A. and Dawe, R.A., 2003. Gas and oil production from waterflood residual oil: effects of wettability and oil spreading characteristics. Journal of Petroleum Science and Engineering, 39(3-4): 297-308.

Grim, R.E., 1953. Clay mineralogy, 76. LWW.

Han, G., Kwon, T.-H., Lee, J.Y. and Jung, J., 2020. Fines migration and pore clogging induced by single-and two-phase fluid flows in porous media: From the perspectives of particle detachment and particle-level forces. Geomechanics for Energy and the Environment, 23: 100131.

Israelachvili, J.N., 2011. Intermolecular and surface forces. Academic press.

Jahanbakhsh, A., Wlodarczyk, K.L., Hand, D.P., Maier, R.R. and Maroto-Valer, M.M., 2020. Review of microfluidic devices and imaging techniques for fluid flow study in porous geomaterials. Sensors, 20(14): 4030.

Karadimitriou, N. and Hassanizadeh, S., 2012. A review of micromodels and their use in two-phase flow studies. Vadose Zone Journal, 11(3): vzj2011. 0072.

Kashiri, R., Kalantariasl, A., Parsaei, R. and Zeinijahromi, A., 2021. Experimental Study of the Effect of Clay and Oil Polarity on Oil Recovery by Low Salinity Water Flooding Using Glass Micromodel. Natural Resources Research: 1-22.

Khajepour, H., Mahmoodi, M., Biria, D. and Ayatollahi, S., 2014. Investigation of wettability alteration through relative permeability measurement during MEOR process: A micromodel study. Journal of Petroleum Science and Engineering, 120: 10-17.

Khilar, K.C. and Fogler, H.S., 1984. The existence of a critical salt concentration for particle release. Journal of colloid and interface science, 101(1): 214-224.

Khilar, K.C. and Fogler, H.S., 1998. Migrations of fines in porous media, 12. Springer Science & Business Media.

Köster, H., 1996. Mineralogical and chemical heterogeneity of three standard clay mineral samples. Clay Minerals, 31(3): 417-422.

Kumari, N. and Mohan, C., 2021. Basics of clay minerals and their characteristic properties. Clay and Clay Minerals: 1-29.

Laroche, C., Vizika, O. and Kalaydjian, F., 1999. Network modeling as a tool to predict three-phase gas injection in heterogeneous wettability porous media. Journal of Petroleum Science and Engineering, 24(2-4): 155-168.

Lebedeva, E.V. and Fogden, A., 2010. Adhesion of oil to KKaolinite in water. Environmental Science & Technology, 44(24): 9470-9475.

Liu, X.D. and Lu, X.C., 2006. A thermodynamic understanding of clay-swelling inhibition by potassium ions. Angewandte Chemie International Edition, 45(38): 6300-6303.

Mackay, E.J., Henderson, G.D., Tehrani, D.H. and Danesh, A., 1998. The importance of interfacial tension on fluid distribution during depressurization. SPE Reservoir Evaluation & Engineering, 1(05): 408-415.

Mahani, H., Berg, S., Ilic, D., Bartels, W.-B. and Joekar-Niasar, V., 2015. Kinetics of low-salinity-flooding effect. SPE Journal, 20(01): 8-20.

Marhaendrajana, T., Ridwan, M.G., Kamil, M.I. and Permadi, P., 2018. Wettability alteration induced by surface roughening during low salinity waterflooding. J Eng Technol Sci, 50(5): 635-649.

Mehdizad, A., Sedaee, B. and Pourafshary, P., 2022. Visual investigation of the effect of clay-induced fluid flow diversion on oil recovery, as a low-salinity water flooding mechanism. Journal of Petroleum Science and Engineering, 209: 109959.

Mohammadalinejad, P., Hosseinpour, N., Rahmati, N. and Rasaei, M.R., 2019. Formation damage during oil displacement by aqueous SiO_2 nanofluids in water-wet/oil-wet glass micromodel porous media. Journal of Petroleum Science and Engineering, 182: 106297.

Mohammadi, M. and Mahani, H., 2020. Direct insights into the pore-scale mechanism of low-salinity waterflooding in carbonates using a novel calcite microfluidic chip. Fuel, 260: 116374.

Mohan, K.K. and Fogler, H.S., 1997. Colloidally induced smectitic fines migration: existence of microquakes. AIChE journal, 43(3): 565-576.

Muhammed, N.S., Olayiwola, T. and Elkatatny, S., 2021. A review on clay chemistry, characterization and shale inhibitors for water-based drilling fluids. Journal of Petroleum Science and Engineering: 109043.

Muneer, R., Hashmet, M.R. and Pourafshary, P., 2020. Fine migration control in sandstones: surface force analysis and application of DLVO theory. ACS omega, 5(49): 31624-31639.

Murray, H.H., 2006. Structure and composition of the clay minerals and their physical and chemical properties. Developments in clay science, 2: 7-31.

Ochi, J. and Vernoux, J.-F., 1998. Permeability decrease in sandstone reservoirs by fluid injection: hydrodynamic and chemical effects. Journal of hydrology, 208(3-4): 237-248.

Oh, Y.S., Jo, H.Y., Ryu, J.-H. and Kim, G.-Y., 2017. A microfluidic approach to water-rock interactions using thin rock sections: Pb and U sorption onto thin shale and granite sections. Journal of Hazardous Materials, 324: 373-381.

Onaka, Y. and Sato, K., 2021. Dynamics of pore-throat plugging and snow-ball effect by asphaltene deposition in porous media micromodels. Journal of Petroleum Science and Engineering, 207: 109176.

Pan, B. et al., 2019. Methane (CH_4) wettability of clay-coated Quartz at reservoir conditions. Energy & fuels, 33(2): 788-795.

Pang, Z. and Liu, H., 2013. The study on permeability reduction during steam injection in unconsolidated porous media. Journal of Petroleum Science and Engineering, 106: 77-84.

Porter, M.L. et al., 2015. Geo-material microfluidics at reservoir conditions for subsurface energy resource applications. Lab on a Chip, 15(20): 4044-4053.

Rahman, M., Suarez, Y., Chen, Z. and Rahman, S., 2007. Unsuccessful hydraulic fracturing cases in Australia: Investigation into causes of failures and their remedies. Journal of Petroleum Science and Engineering, 57(1-2): 70-81.

Ridwan, M.G. et al., 2020. Low salinity waterflooding: Surface roughening and pore size alteration implications. Journal of Petroleum Science and Engineering, 195: 107868.

Rogala, A., Krzysiek, J., Bernaciak, M. and Hupka, J., 2013. Non-aqueous fracturing technologies for shale gas recovery. Physicochemical Problems of Mineral Processing, 49.

Saadat, M., Yang, J., Dudek, M., Øye, G. and Tsai, P.A., 2021. Microfluidic investigation of enhanced oil recovery: The effect of aqueous floods and network wettability. Journal of Petroleum Science and Engineering, 203: 108647.

Sarkar, A.K. and Sharma, M.M., 1990. Fines migration in two-phase flow. Journal of petroleum technology, 42(05): 646-652.

Sayegh, S., Krause, F., Girard, M. and DeBree, C., 1990. Rock/fluid interactions of carbonated brines in a sandstone reservoir: Pembina Cardium, Alberta, Canada. SPE Formation Evaluation, 5(04): 399-405.

Schembre, J., Tang, G.-Q. and Kovscek, A., 2006. Wettability alteration and oil recovery by water imbibition at elevated temperatures. Journal of Petroleum Science and Engineering, 52(1-4): 131-148.

Seyyedi, M., Mahzari, P. and Sohrabi, M., 2018. A comparative study of oil compositional variations during CO_2 and carbonated water injection scenarios for EOR. Journal of Petroleum Science and Engineering, 164: 685-695.

Shahmohammadi, B., Chahardowli, M. and Simjoo, M., 2021. Insights into the pore-scale mechanism of low salinity water injection using a clay-coated micromodel. Journal of Petroleum Science and Engineering: 110065.

Shaik, I.K., Aichele, C.P. and Bikkina, P.K., 2022. Microfluidics-Based Low Salinity Wettability Alteration Study of Naphthenic-Acid-Adsorbed Calcite Surfaces. Energy & Fuels.

Shaik, I.K. et al., 2020. A parametric study of layer-by-layer deposition of $CaCO_3$ on glass surfaces towards fabricating carbonate reservoirs on microfluidic chips. Journal of Petroleum Science and Engineering: 108231.

Sharifipour, M., Nakhaee, A. and Pourafshary, P., 2019. Model development of permeability impairment due to clay swelling in porous media using micromodels. Journal of Petroleum Science and Engineering, 175: 728-742.

Shaw, D.B. and Weaver, C.E., 1965. The mineralogical composition of shales. Journal of Sedimentary Research, 35(1): 213-222.

Siadatifar, S.E., Fatemi, M. and Masihi, M., 2021. Pore scale visualization of fluid-fluid and rock-fluid interactions during low-salinity waterflooding in carbonate and sandstone representing micromodels. Journal of Petroleum Science and Engineering, 198: 108156.

Smith, J.D., Chatzis, I. and Ioannidis, M.A., 2005. A new technique to measure the breakthrough capillary pressure. Journal of Canadian Petroleum Technology, 44(11).

Shehata, A.M. and Nasr-El-Din, H.A., 2015. Zeta potential measurements: Impact of salinity on sandstone minerals, SPE International Symposium on Oilfield Chemistry. OnePetro.

Somerton, W. and Radke, C., 1983. Role of clays in the enhanced recovery of petroleum from some California sands. Journal of Petroleum Technology, 35(03): 643-654.

Song, W. and Kovscek, A.R., 2015. Functionalization of micromodels with KKaolinite for investigation of low salinity oil-recovery processes. Lab on a Chip, 15(16): 3314-3325.

Song, W. and Kovscek, A.R., 2016. Direct visualization of pore-scale fines migration and formation damage during low-salinity waterflooding. Journal of Natural Gas Science and Engineering, 34: 1276-1283.

Środoń, J., 1999. Nature of mixed-layer clays and mechanisms of their formation and alteration. Annual Review of Earth and Planetary Sciences, 27(1): 19-53.

Stephens, M., Gomez-Nava, S. and Churan, M., 2009. Laboratory methods to assess shale reactivity with drilling fluids, AADE National Technical Conference, New Orleans.

Su, Y. et al., 2022. Experimental study on microscopic mechanisms and displacement efficiency of N_2 flooding in deep-buried clastic reservoirs. Journal of Petroleum Science and Engineering, 208: 109789.

Sun, Z., Pu, W., Zhao, R. and Pang, S., 2021. Study on the mechanism of W/O emulsion flooding to enhance oil recovery for heavy oil reservoir. Journal of Petroleum Science and Engineering: 109899.

839 Tangparitkul, S., Saul, A., Leelasukseree, C., Yusuf, M. and Kalantariasl, A., 2020. Fines
840 migration and permeability decline during reservoir depletion coupled with clay swelling
841 due to low-salinity water injection: An analytical study. Journal of Petroleum Science and
842 Engineering, 194: 107448.

843 Tchistiakov, A.A., 2000. Colloid chemistry of in-situ clay-induced formation damage, SPE
844 International Symposium on Formation Damage Control. OnePetro.

845 Wilson, L., Wilson, M., Green, J. and Patey, I., 2014. The influence of clay mineralogy on
846 formation damage in North Sea reservoir sandstones: a review with illustrative examples.
847 Earth-Science Reviews, 134: 70-80.

848 Xu, L., Han, M., Cao, D. and Wang, J., 2022. Study on dynamic interfacial tension behaviors in
849 surfactant selection for improving oil production. Journal of Petroleum Science and
850 Engineering, 209: 109978.

851 Yekeen, N., Padmanabhan, E., Syed, A.H., Sevoo, T. and Kanesen, K., 2020. Synergistic
852 influence of nanoparticles and surfactants on interfacial tension reduction, wettability
853 alteration and stabilization of oil-in-water emulsion. Journal of Petroleum Science and
854 Engineering, 186: 106779.

855 Zeinijahromi, A., Lemon, P. and Bedrikovetsky, P., 2011. Effects of induced fines migration on
856 water cut during waterflooding. Journal of Petroleum Science and Engineering, 78(3-4):
857 609-617.

858 Zhang, Y., Sanati-Nezhad, A. and Hejazi, S., 2018. Geo-material surface modification of
859 microchips using layer-by-layer (LbL) assembly for subsurface energy and
860 environmental applications. Lab on a Chip, 18(2): 285-295.

861 Zhuang, Y., Liu, X., Xiong, H. and Liang, L., 2018. Microscopic mechanism of clay minerals on
862 reservoir damage during steam injection in unconsolidated sandstone. Energy & Fuels,
863 32(4): 4671-4681.

864